Composite Structures 281 (2022) 114982

Contents lists available at ScienceDirect

Composite Structures

journal homepage: www.elsevier.com/locate/compstruct

Experimental and finite element studies on the structural behavior of BFRC continuous beams reinforced with BFRP bars

Abdelrahman Abushanab, Wael Alnahhal *, Murad Farraj

[a] Department of Civil and Architectural Engineering, College of Engineering, Qatar University, Doha, Qatar

ARTICLE INFO

Keywords:
Continuous beams
Finite element analysis
Moment redistribution
Fiber-reinforced concrete
BFRP bars
Basalt macro-fibers

ABSTRACT

This study presents an experimental and numerical study on the structural behavior and moment redistribution of basalt fiber-reinforced concrete (BFRC) continuous beams with basalt fiber-reinforced polymer (BFRP) bars. A total of seven BFRP-BFRC two-span continuous beams were tested to failure under a five-point test setup. Three parameters were investigated: volume fractions (V_f) of basalt macro-fibers (BMF), BFRP reinforcement ratio, and stirrups spacing. Test results indicated that compared to stirrups spacing, reinforcement ratio and V_f of BMF were more significant in improving the structural performance and moment redistribution of the tested beams. Furthermore, nonlinear 2D finite element (FE) models were developed using the commercial ABAQUS software to predict the behavior of the tested beams. The FE analysis accounted for the tensile cracking and compressive crushing of concrete using the built-in concrete damaged plasticity model. Ayub's analytical model was employed to simulate the nonlinearity of BFRC in compression. The accuracy of the FE models was validated using the experimental load-deflection responses and crack patterns at failure. Good agreement was obtained between the experimental and numerical results with the experimental-to-predicted mean, standard deviation, and coefficient of variance values of 1.036, 0.041, and 3.95% for the ultimate loads and 0.993, 0.046, and 4.68% for the deflections, respectively.

1. Introduction

Fiber-reinforced polymer (FRP) bars have attracted immense attention as a viable non-corrosive alternative to conventional steel bars in reinforced concrete (RC) structures. FRP bars are characterized by their superior corrosion resistance and less weight-to-strength ratio and lower life-cycle cost than traditional steel reinforcements [1]. More recently, basalt FRP (BFRP) bars have evolved as a promising alternative to the commercialized glass FRP (GFRP) bars because of their cost-effectiveness, comparable tensile strength, and better chemical and alkali resistance [2,3]. The majority of the previous studies have focused only on the structural performance of BFRP-RC simply-supported beams and slabs [2,4–9] and BFRP bond to concrete [10–17]. Nevertheless, there is a lack of knowledge concerning the structural behavior and moment redistribution of BFRP-RC continuous beams despite the fact that RC continuous beams are the most widely used structural element.

The structural performance of steel-RC continuous beams and their efficiency in redistributing forces between sagging and hogging sections is well understood and extensively documented in the literature [18–21]. Recently, a number of research studies were conducted on the structural behavior of carbon FRP (CFRP) and GFRP-RC continuous beams [22–27]. However, little data are available on the structural performance of BFRP-RC continuous slabs and beams [28,29].

Even though the moment redistribution enhances the ductility and rotational capacities of RC continuous beams, it is still exempted from the available FRP design codes and guidelines [30–33] because of the FRPs' brittleness. Nonetheless, several researchers have demonstrated that FRP-RC continuous beams exhibit a uniform moment redistribution similar to their counterparts with steel reinforcement [24,26–28,34–36]. For instance, Akiel et al. [28], Habeeb and Ashour [24], El-Mogy et al. [26], and Santos et al. [37] revealed that the moment redistribution of FRP-RC continuous beams depends on the longitudinal reinforcement ratio. According to their studies, the beams with higher sagging-to-hogging reinforcement ratios reported higher moment redistribution. Furthermore, Rahman et al. [34] showed that RC continuous beams with closer stirrups spacing recorded higher moment redistribution. However, El-Mogy et al. [25] reported that the moment redistribution in FRP-RC beams is affected by the stirrups

* Corresponding author.
E-mail addresses: aa1104287@qu.edu.qa (A. Abushanab), wael.alnahhal@qu.edu.qa (W. Alnahhal), mf1606873@qu.edu.qa (M. Farraj).

https://doi.org/10.1016/j.compstruct.2021.114982
Received 24 March 2021; Accepted 9 November 2021
Available online 14 November 2021

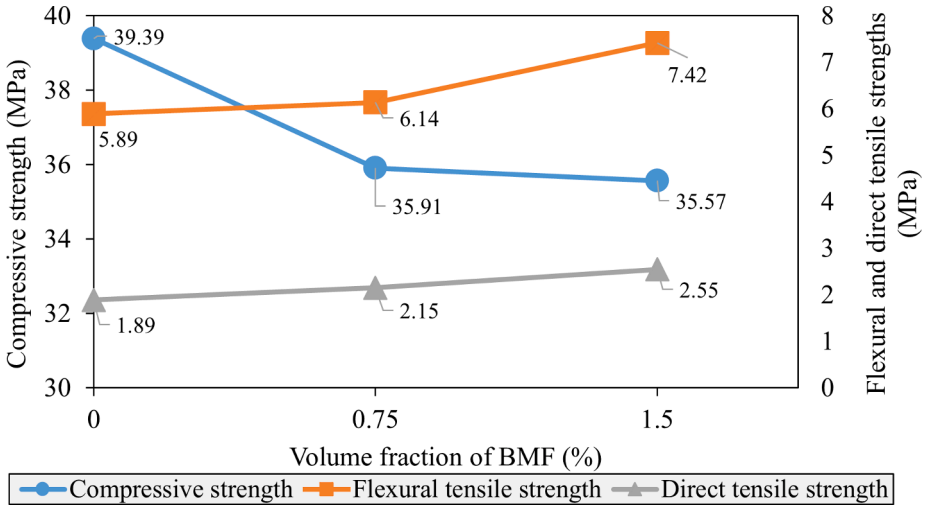

Fig. 1. Average compressive, flexural, and tensile strengths with different V_f of BMF.

diameter, not stirrups spacing. Mahroug et al. [29] demonstrated that the moment redistribution of BFRP-RC continuous slabs likely occurred because of the variation of the flexural stiffness of the slabs, debonding of BFRP bars from surrounding concrete, and concrete cracks. On the other hand, only one study has examined the moment redistribution of BFRP-RC continuous beams. In their study, Akiel et al. [28] showed that RC beams with BFRP bars achieved higher moment redistribution than those with a hybrid combination of BFRP and steel bars. Furthermore, Akiel et al. [28] reported that increasing the hogging-to-sagging reinforcement ratio increased the flexural rigidity of the hogging section and consequently decreased the moment redistribution.

On the other hand, FRP bars show a linear elastic behavior up to failure and have lesser ductility than steel bars, which is a downside when used as in RC beams. Addressing this concern, several researchers have explored the possibility of using fiber-reinforced concrete (FRC) with FRP-RC structures [2,38–42]. The addition of fibers to the concrete mixture mainly increases the ultimate compressive strain of concrete, thereby enhancing the rotational capacity of the FRP-reinforced members. This unique characteristic of the FRC is of great significance when FRP bars are used as internal reinforcement in continuous beams as it enhances their moment redistribution. Yang et al. [38] reported that the incorporation of synthetic and steel discrete fibers in concrete increased the first cracking load and improved the ductility index of FRP-RC beams. Wang and Belarbi [43] also revealed that the FRP-RC beams with discrete polypropylene fibers achieved lower crack widths and higher ductility index than those with no fibers. Attia et al. [2], Abed and Alhafiz [44], and Lee et al. [45] have also reported similar results. Furthermore, Visintin et al. [46] demonstrated that moment redistribution of FRC continuous beams started even before their plastic limits. Nevertheless, the addition of steel fibers to concrete mixes might deteriorate and adversely affect the performance of RC members because of their high iron content and corrosiveness [2]. This study, therefore, addressed the feasibility of replacing steel fibers with non-corrosive basalt macro-fibers (BMF). In addition to their non-corrosiveness, basalt fibers are characterized by their higher elastic modulus than other synthetic fibers [47]. Abed and Alhafiz [44] observed that the moment capacity of BFRP-BFRC beams increased by increasing the volume fractions (V_f) of BMF. Thus far, studies on the effect of BMF on the structural behavior and moment redistribution of continuous beams with BFRP bars have not been reported. Therefore, this study was conducted to fill the gap in the literature.

On the other hand, with the recent advances in computational technology, the finite element method (FEM) has become an essential and inexpensive tool to simulate the behavior of RC elements under various geometric and loading conditions. Modeling the nonlinear response of concrete is one of the most challenging aspects of FEM simulations. Considering the elasticity, plasticity, and concrete damage theories, different constitutive models for concrete have been adapted by FEM software [48]. Numerous researchers have numerically simulated the structural performance of FRP-RC elements [5,49–53]. For instance, Cai et al. [5] created a finite element (FE) model to study the performance of BFRP-RC simply supported beams using ATENA/GID software. The authors [5] have employed the fracture-plastic model to simulate concrete behavior, whereas reinforcing bars were modeled using truss elements. Good agreement with the experimental results was achieved in terms of failure modes and load–deflection responses. Pawłowski and Szumigała [52] performed numerical studies on BFRP-RC simply supported beams using ABAQUS software. In their study [52], tension stiffening of concrete was simulated using Wang and Hsu modified formula [54]. Thus far, numerical studies and simulations have only focused on simply supported RC beams and slabs prepared with conventional concrete. Nonetheless, marginal attention has been focused on FRP-FRC continuous members.

In this study, the structural behavior and moment redistribution of BFRP-BFRC continuous beams were experimentally and numerically investigated. Three parameters were investigated, namely V_f of BMF, BFRP reinforcement ratio, and stirrups spacing. Moreover, a two-dimensional (2D) FE model using ABAQUS software was developed and calibrated. The sensitivity of the FE model was provided. The developed model was validated against the experimental results of the tested beams. Additional research on a broader range of parameters could be implemented by the FE models developed in this study as alternatives to the laboratory tests.

2. Materials and methods

2.1. Material properties

2.1.1. Concrete mixes

Three ready-mix concrete patches made with three V_f of BMF (0, 0.75, and 1.5%) with a target 28-day compressive strength of 35 MPa were used in this study. BFRC slump was immediately determined after casting as per ASTM C143/C143M-15a provisions [55]. Slump test results revealed that concrete slump was slightly affected by the addition of the BMF. Plain concrete reported a slump of 180 mm, whilst BFRC at V_f of 0.75% and 1.5% had a slump of 160 and 150 mm, respectively. This reduction might have occurred because of the larger surface area of BMF, which absorbed part of the cement paste and thus increased concrete's viscosity [56]. These results are similar to those reported by Ramesh and Eswari [57]. Compressive and flexural tensile strengths for

(a) (b)

Fig. 2. Failure of flexural strength test prisms: (a) plain prism and (b) BFRC prism.

the three concrete patches were measured at 28 days in accordance with ASTM C39/C39M-20 [58] and ASTM C1609/C1609M-12 provisions [59], respectively. As shown in Fig. 1, the compressive strength was slightly affected by adding BMF. BFRC specimens at V_f of 0.75% and 1.50% recorded about 9% lower compressive strength than plain concrete specimens. This might be attributed to the larger surface area of BMF, which alerted the macrostructure of concrete and increased entrapped air in the matrix. On the other hand, test results showed that BMF significantly improved BFRC flexural tensile strength. Fig. 1 shows that BFRC specimens at V_f of 1.5% achieved 25% higher flexural tensile strength than plain specimens. Moreover, adding BMF to concrete has changed the failure mode of the flexural prisms from a brittle failure (Fig. 2(a)) to a more ductile one (Fig. 2(b)). That was due to the bridging effect of BMF, which bridged the initiated cracks at BFRC surfaces and redistributed the tensile stresses along the entire prisms' lengths. Similar results were also reported by Attiaa et al. [2], Jiang et al. [60], and Branston et al. [61].

Concrete direct tensile strength was measured at 28 days using three "I" shaped specimens with a layout and dimensions shown in Fig. 3(a). The "I" specimens were reinforced with 8-mm steel bars at both squares to ensure a neck failure. The specimens were also provided with two holes at the square areas to be safely mounted on the Universal Testing Machine (UTM) (Fig. 3(b)). It could be noticed from Fig. 1 that adding BMF at V_f of 0.75% and 1.5% increased the direct tensile strength by 14% and 35% in comparison with plain concrete specimens, respectively. The effect of the BMF could also be observed in the tensile stress–strain curves in Fig. 4. Plain specimens had a sudden and abrupt drop at failure, whilst BFRC specimens experienced a more progressive failure and restrained 43% and 38% of the tensile strength at V_f of BMF of 0.75% and 1.5%, respectively, until BMF pullout or rupture. This is attributed to the bridging effect of the BMF, which absorbed the tensile stresses and prevented the propagation of internal cracks. Such improvements in BFRC specimens indicated that BMF increased concrete ductility. Similar trends were also observed by Attia et al. [2] and Alnahhal and Aljidda [62].

Thickness = 100 mm

(a)

(b)

Fig 3. Direct tensile strength test: (a) specimens' dimensions, layout, and formwork and (b) test setup.

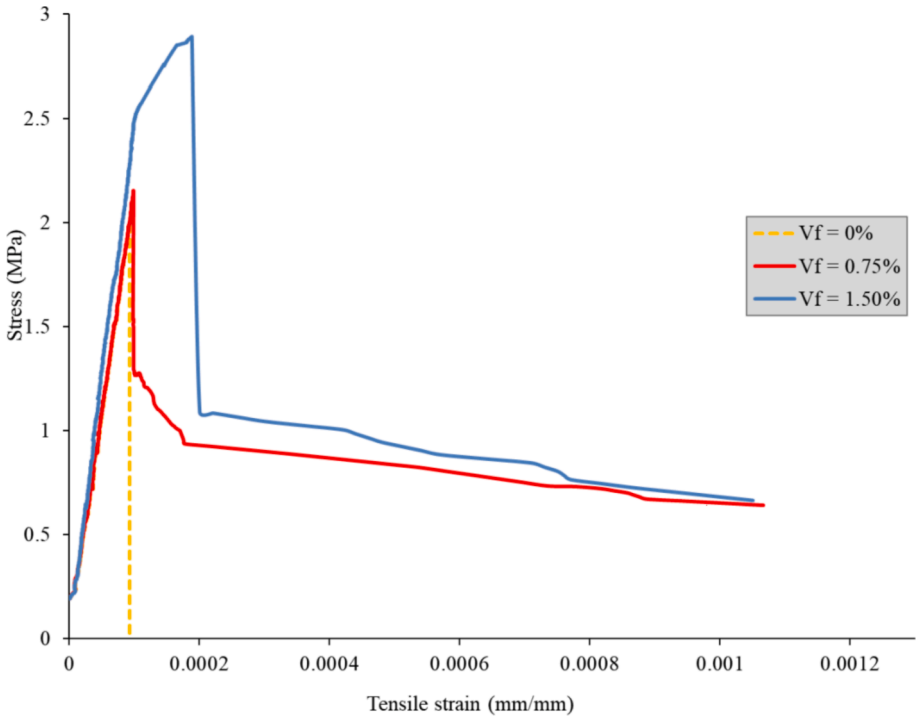

Fig. 4. Stress–strain curves of direct tensile test specimens with different V_f of BMF.

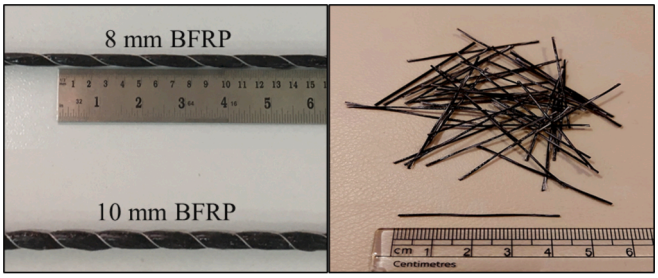

Fig. 5. Reinforcement used in this study: (a) BFRP bars and (b) BMF.

Table 1
Properties of steel and BFRP reinforcement.

Reinforcement material	ϕ10-steel stirrup	ϕ10-BFRP bar	ϕ8-BFRP bar
Modulus of elasticity (GPa)	195	44.7	42.7
Yielding tensile strength (MPa)	515	N.A	N.A
Yield strain (mm/mm)	0.00268	N.A	N.A
Ultimate tensile strength (MPa)	553	1070	1096
Ultimate strain (mm/mm)	0.248	0.023	0.027

Note: N.A = Not applicable.

2.1.2. BFRP and steel reinforcement

BFRP bars with diameters of 8 and 10 mm were used in this study as the beams' main reinforcement (Fig. 5(a)). The BFRP bars have a helical wrapping surface with an indentation distance of 3 cm to improve the interlocking and bonding mechanism with concrete. All beams were made of 10-mm diameter steel stirrups. Table 1 lists the properties of steel and BFRP reinforcement, as provided by the manufacturers.

2.1.3. Basalt macro-fibers

BMF, shown in Fig. 2(b), had a length of 43 mm, diameter of 0.66 mm, specific gravity of 1.9 g/cm^3, elastic modulus of 44 GPa, ultimate tensile strength of 1100 MPa, and ultimate strain of 0.021. The BMF used have a rough and helical surface texture to improve interlocking and bonding mechanism with the surrounding concrete.

2.2. Continuous RC beam details and test setup

Seven two-span continuous RC beam specimens were tested in order to validate the developed finite element models. The geometry, reinforcement arrangement, and loading patterns of the tested beams are shown in Fig. 6. Three parameters were considered, namely V_f of BMF (0%, 0.75%, and 1.5%), sagging-to-hoggin reinforcement ratio (0.32, 0.67, 1.00, 1.33, and 1.50), and stirrups spacing (80 and 120 mm). Table 2 presents a detailed testing matrix for the beam specimens. The beams' designation is summarized in Fig. 7. The beams were designed according to the procedures stipulated in ACI 440.1R-15 guidelines [30]. All tested beams were designed for flexural failure except beams V1-R4-S1, V2-R4-S1, and V3-R4-S1 designed for shear failure to evaluate the moment redistribution in shear failure mode and to examine the effect of the BMF in resisting the shear forces.

The details of the test setup and instrumentations of a typical continuous beam specimen are illustrated in Fig. 8. All tests were carried out using a constant displacement rate of 1 mm/min. The support reactions were monitored using load cells placed under the support locations. Linear variable differential transducers (LVDTs) were added at both midspans to measure the mid-span deflections. Strain gauges were bonded at concrete and reinforcement surfaces to measure concrete and reinforcement strains. Furthermore, a 200-mm-long crack transducer was placed at the hogging middle support to measure the crack widths.

3. The numerical simulation

3.1. Model description

Seven FE models representing the seven tested beams were developed using ABAQUS 6.14 commercial software [63]. A number of researchers have implemented ABAQUS software to simulate the

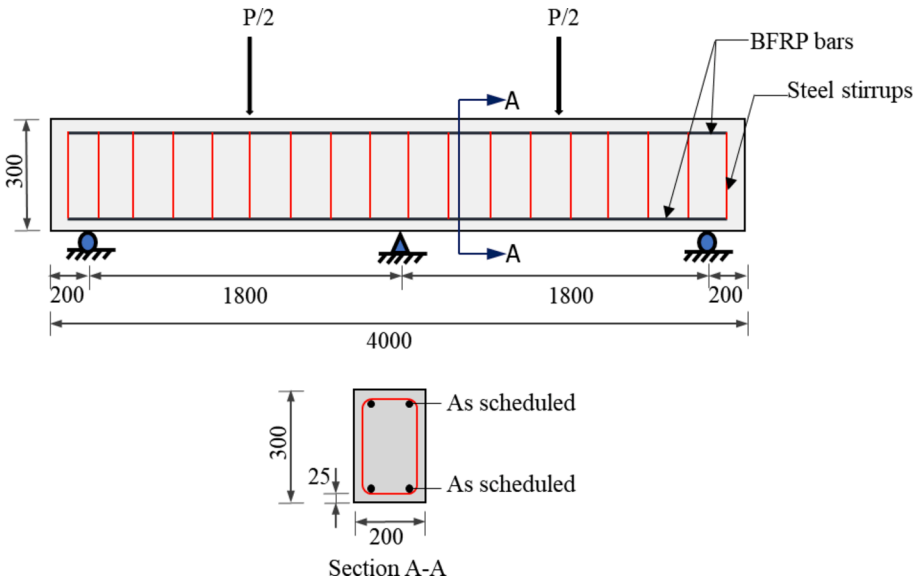

Fig. 6. Geometry, main reinforcement details, and loading patterns of the tested beams (all dimensions are in mm).

Table 2
Testing matrix of the beams.

Beam	V_f of BMF	Sagging reinforcement	Hogging reinforcement	Sagging reinforcement ratio (ρ/ρ_{bf})	Hogging reinforcement ratio (ρ/ρ_{bf})	Sagging-to-hoggin reinforcement ratio	Transverse reinforcement spacing (mm)
V1-R4-S1	0.00%	6 ϕ 10	4 ϕ 10	3.69	2.33	1.50	120
V2-R4-S1	0.75%	6 ϕ 10	4 ϕ 10	3.87	2.45	1.50	120
V3-R4-S1	1.50%	6 ϕ 10	4 ϕ 10	3.88	2.46	1.50	120
V1-R4-S2	0.00%	6 ϕ 10	4 ϕ 10	3.69	2.33	1.50	80
V2-R3-S1	0.75%	6 ϕ 10	6 ϕ 10	3.87	3.87	1.00	120
V2-R2-S1	0.75%	4 ϕ 10	6 ϕ 10	2.45	3.87	0.67	120
V2-R1-S1	0.75%	2 ϕ 8	4 ϕ 10	0.8	2.45	0.32	120

Note. ρ_{bf} = balance reinforcement ratio as per ACI 440.1R-15 guidelines [29].

nonlinear behavior of steel and FRP-RC elements with a good matching between the experimental and numerical results [64–67]. ABAQUS software provides three constitutive models for concrete modeling, namely concrete brittle cracking (CBC), concrete smeared cracking (CSM), and concrete damaged plasticity (CDP) [63]. Both CBC and CSM

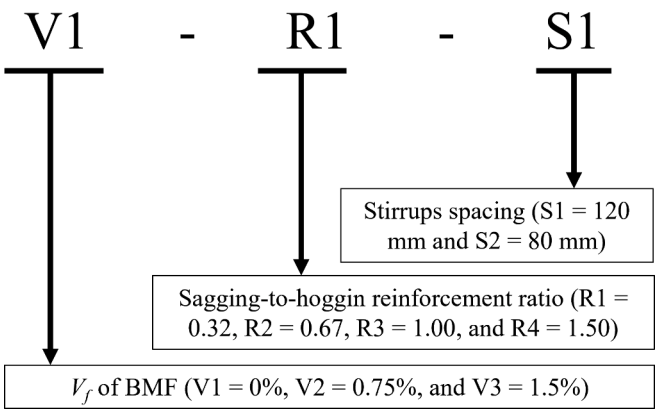

Fig. 7. Designation of the tested beams.

models are unfit for concrete, as the CBC model simulates only the tensile behavior of concrete, and the CSC model causes stress allocation at open cracks and is unstable at higher loadings [48]. The CDP, however, simulates the tension and compression failure modes of concrete, can be subjected to monotonic, cyclic, and dynamic loadings, and considers concrete's permanent strains resulting from the loading and unloading stages [63]. Several studies have successfully employed the CDP model in FRP-RC elements and obtained comparable results to that obtained experimentally [48,52,64,68–70]. In this study, the full-length beam model was constructed to provide a uniform loading condition and to consider unsymmetrical loading patterns for future studies. Moreover, the FE models were constructed in 2D to reduce computational time. Material nonlinearity was also adapted in the constructed FE model to accurately simulate the beams' behavior. BFRC element was modeled as a 4-node 2D solid homogeneous element, while both steel and BFRP reinforcements were modeled as a 2-node 1D truss element. None of the tested beams had a bond failure. Therefore, all FE models were constructed with a perfect bond between concrete and the embedded BFRP bars and steel stirrups. All simulated beams were loaded with a vertical displacement of 1 mm/step to failure. The loads and displacements were reported at each step. Further information related to the element types employed in the current study can be found in ABAQUS 6.14 user's manual [63]. The following subsections discuss the element types, geometry, and modeling procedures of the constructed FE beam models in detail.

3.2. Element types

3.2.1. BFRC

The build-in CDP model was used to model plain concrete and BFRC elements as a 4-node 2D solid homogeneous element [63]. The properties of the CDP model used in this study are listed in Table 3.

BFRC compressive stress–strain response was modeled using Ayub et al. [71] analytical model. As can be noticed in Fig. 9 and Table 4, the

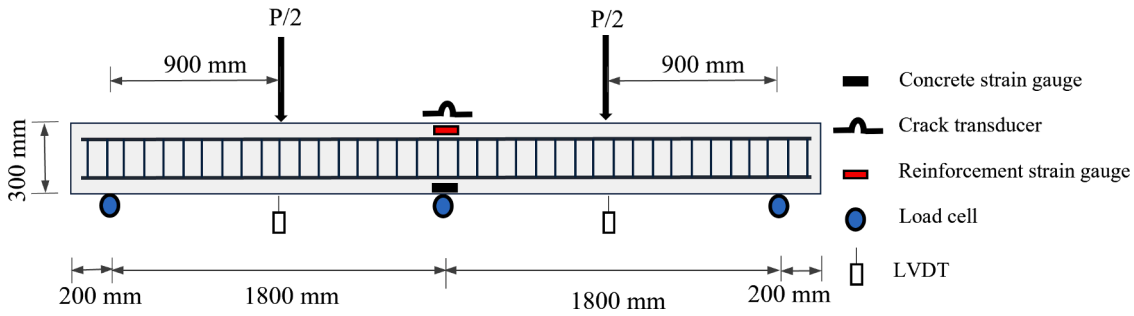

Fig. 8. Test setup and instrumentations of a typical beam specimen.

Table 3
Properties of the CDP model.

Property	Value
Poisson's ratio ν	0.18
Dilation angle φ	20.0
Eccentricity ε	0.10
σ_{bo}/σ_{co}	1.16
Concrete density ρ (kN/m^3)	25.0

Note: σ_{bo}/σ_{co} = the ratio of initial biaxial compressive to the initial uniaxial compressive yield stress

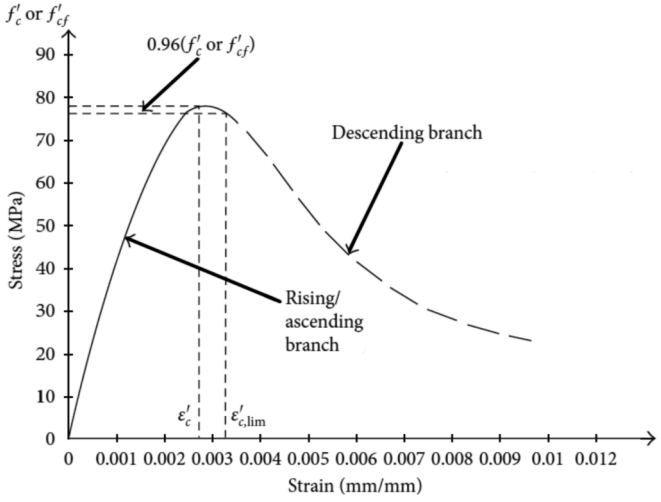

Fig. 9. Compressive stress–strain of BFRC (Ayub et al. [71]).

model consists of two coupled equations: Eq. (1) that describes the stress–strain response up to $f_c = 0.96 \times f_c^{'}$ and Eq. (2) that measures the impact of the BMF after the failure (i.e., $f_c > 0.96 \times f_c^{'}$). Eqs. (1) and (2) are represented in Fig. 9 as the ascending and descending branches, respectively.

Up to date, there is no globally accepted analytical formula to predict the tensile stress–strain response of BFRC. For that reason, the experimental BFRC tensile stress–strain response for V_f of 0%, 0.75%, and 1.5%, shown in Fig. 4, was used in the developed FE models.

3.2.2. Steel and BFRP elements

Both steel and BFRP elements were modeled as a 2-node 1D truss element. The truss element simulates the elastic and plastic deformations of the reinforcing bars. As per ABAQUS user's manual [63], the truss element has one axial degree of freedom per node. The elastic part of the steel reinforcement is defined by Poisson's ratio and elastic modulus, while the yielding stress and inelastic strain define the plastic part. The mechanical properties of BFRP and steel reinforcements are presented in Table 1. The BFRP element was defined as a linear stress–strain relationship until failure, whilst steel element as a bilinear stress–strain relationship.

3.3. Geometric modeling of the FE model

The geometric, loading patterns, element types, and boundary conditions of the developed FE models were identical to the tested beams, as shown in Fig. 10. The 2D geometric model was preferred over the 3D model because the torsional effect was not considered in this study and to reduce computational time. Rigid bodies with a capacity of 90 GPa (shown in brown color in Fig. 10) were modeled under the applied load locations and at both overhangs. These bodies were modeled to avoid any stress concentration under the load locations and to neglect the

Table 4
Equation used in predicting the compressive stress–strain of the BFRC (Ayub et al. [71]).

Model	Relevant formula
$f_c = \frac{n\beta f_c^{'}(\frac{\varepsilon_{cf}}{\varepsilon_{of}})}{n\beta - 1 + (\frac{\varepsilon_{cf}}{\varepsilon_{of}})^{n\beta}} 0 < \varepsilon_{cf} \le \varepsilon_{cf,lim}$ (1)	$\beta = \left(\frac{f_c^{'}}{65.23}\right)^3 + 2.59$ (For plain concrete) (4)
$f_{cf} = f_{cf,lim} \times exp\left[\left(1 - n + 0.1V_f^2\right) \times \left\{\frac{\varepsilon_{cf}}{\varepsilon_{of}} - \frac{\varepsilon_{cf,lim}}{\varepsilon_{of}}\right\}^{1-0.1V_f}\right] \varepsilon_{cf} \ge \varepsilon_{cf,lim}$ (2)	$\beta = \frac{1}{\left(1 - \left(\frac{E_{cf}}{E_{it}}\right)\right)}$ (For BFRC) (5)
$f_{cf,lim} = 0.96 \times f_c^{'}$ (3)	$E_{it} = (10300 - 400V_f)\sqrt{3f_c^{'}}$(MPa) (6)
	$E_{cf} = \frac{f_c^{'}}{\varepsilon_{of}}$ (7)
n = constant related to curve toughness β = constant related to curve shape $f_c^{'}$ = concrete compressive strength, (MPa) ε_{cf} = strain at the concrete stress of f_c ε_{of} = strain at concrete stress of $f_c^{'}$ V_f = V_f of BMF	E_{it} = initial modulus of elasticity, (MPa) E_{cf} = final modulus of elasticity, (MPa)

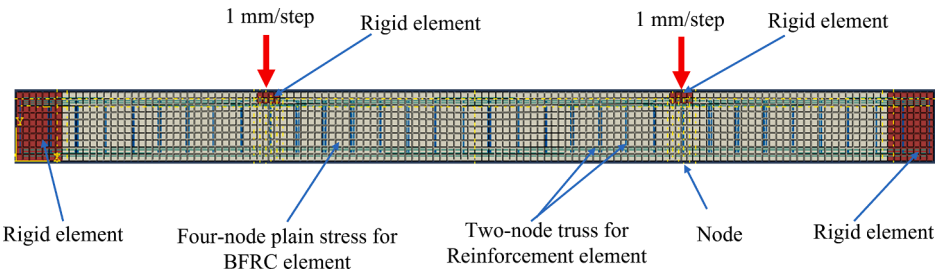

Fig. 10. Geometric, loading patterns, element types, and node locations of the developed FE model.

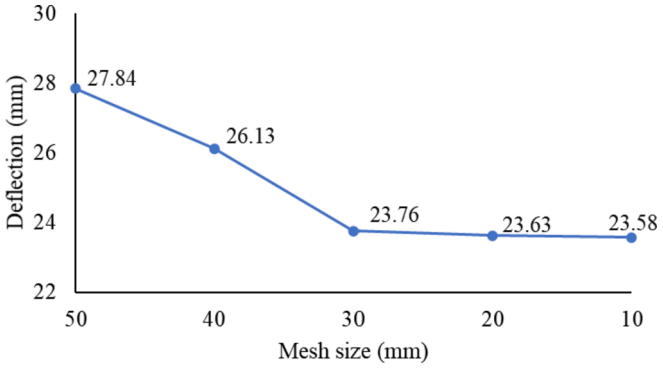

Fig. 11. Effect of mesh size on the FE accuracy.

Table 5
Mode of failure and mid-span deflection at failure of all tested beam.

Beam	Failure mode	Maximum mid-span deflection
V1-R4-S1	shear	23.48
V2-R4-S1	concrete crushing	22.56
V3-R4-S1	concrete crushing	20.34
V1-R4-S2	concrete crushing	23.09
V2-R3-S1	concrete crushing	26.06
V2-R2-S1	concrete crushing	28.59
V2-R1-S1	BFRP bar rupture	10.65

contribution of both overhangs in the beams' stiffness. Furthermore, seven nodes (shown in yellow color in Fig. 10) were created: three at support reactions, two at both midspans, and two at the applied load locations. These nodes were used to record the support reactions, mid-span deflections, and loads. The support reactions included two roller supports at both ends and one pin support at the middle. The pin support was restrained in both vertical and horizontal directions, while the roller support was restrained only in the vertical direction.

3.4. Solution and convergence criteria

The convergence of the FE model was achieved by conducting a mesh size sensitivity study on five FE models for beam V1-R4-S2. The loading was performed at a displacement rate of 1 mm/step until failure. The mesh sizes considered ranged between 10 and 50 mm. The effect of mesh size on the FE models in terms of the mid-span deflection at ultimate load is presented in Fig. 11. After running these FE models, it was noticed that FE models with a mesh size smaller than 30 mm had significantly higher computational time without significantly improving the models' accuracy. Therefore, the FE model with a mesh size of 30 mm was considered in this study.

4. Results and discussion

4.1. Experimental test results

All beams were gradually loaded to failure under a five-point test setup. The failure mode and mid-span deflection at failure are presented

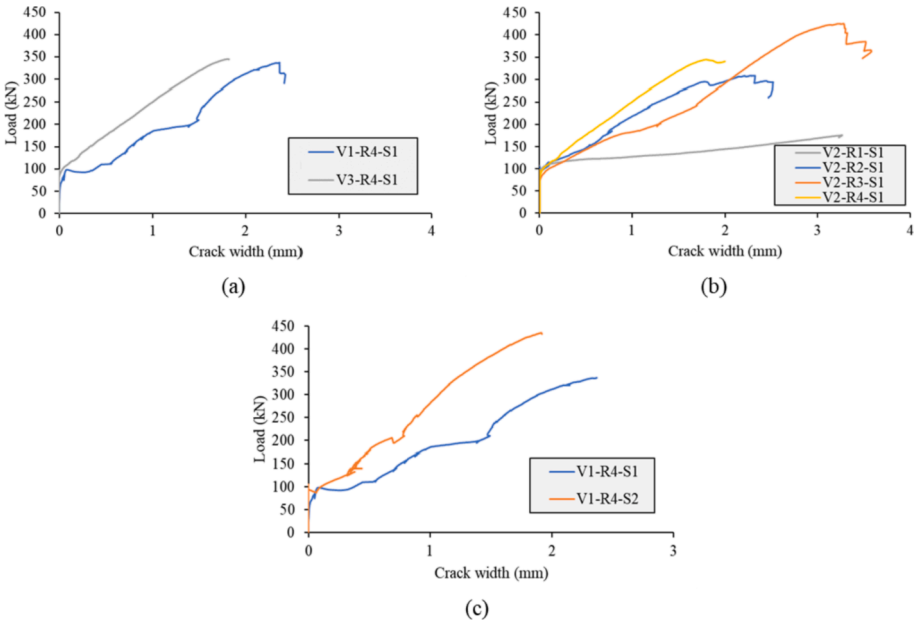

Fig. 12. Load versus crack width with different: (a) V_f of BMF, (b) sagging-to-hogging reinforcement ratio, and (c) stirrups spacing.

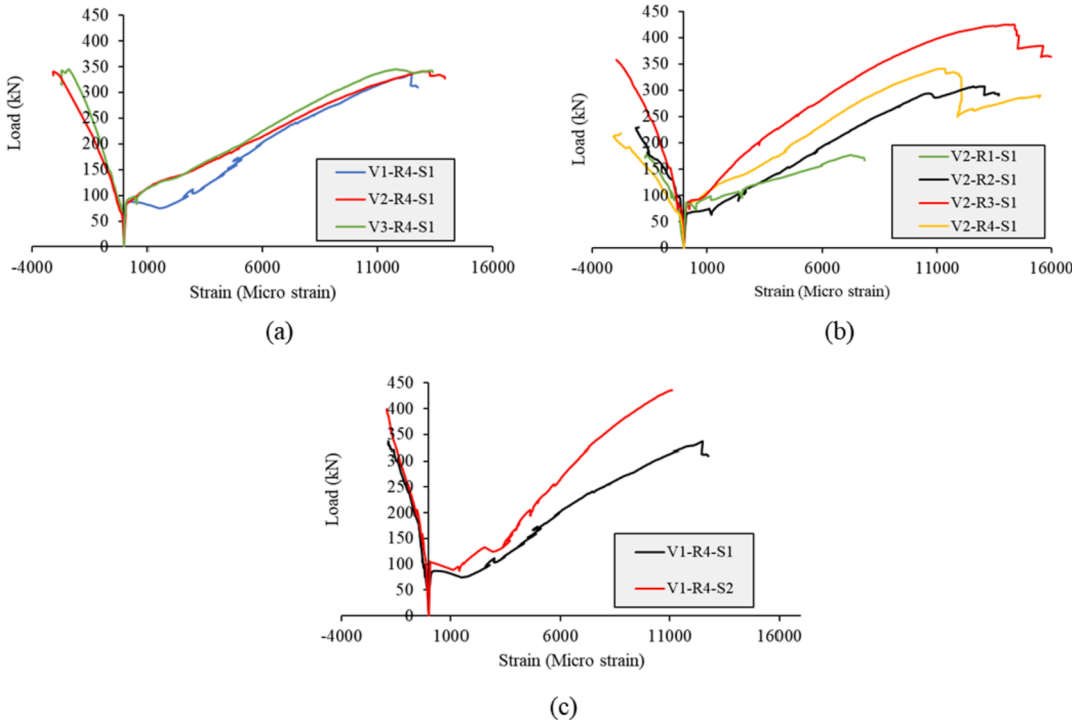

Fig. 13. Effect of the measured concrete and reinforcing bar strains with: (a) V_f of BMF, (b) sagging-to-hogging reinforcement ratio, and (c) stirrups spacing.

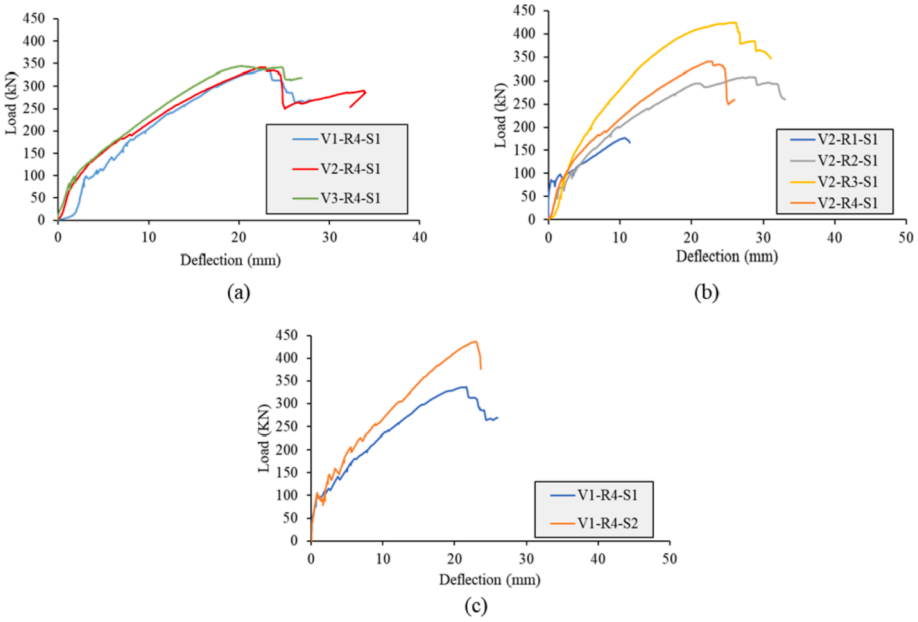

Fig. 14. Effect of the measured mid-span deflections with (a) V_f of BMF, (b) sagging-to-hogging reinforcement ratio, and (c) stirrups spacing.

in Table 5. The tested beams exhibited three failure modes: concrete crushing, BFRP bar rupture, and shear failure. Detailed discussion on the effect of BMF, reinforcement ratio, and stirrups spacing on the tested beams' crack widths, strains, deflections, load-carrying capacity, end-reaction deviations, and moment redistribution are presented in the following subsections.

4.1.1. *Effect of BMF*

Test results indicated that the addition of BMF controlled the propagation and widening of cracks and improved the beams' failure mode. For instance, beam V1-R4-S1 exhibited a diagonal-shear crack at the middle of the beam. As the loads increased, the diagonal crack widened and propagated toward the compression zone of the beam, and thus the beam failed in shear failure mode. Nevertheless, adding BMF in beams V2-R4-S1 and V3-R4-S1 has restrained the widening and propagation of the shear cracks and prevented the shear failure. Consequently, both beams V2-R4-S1 and V3-R4-S1 failed by a flexural-compression failure mode (i.e., concrete crushing). It could also be observed from Fig. 12(a) that adding 1.5% V_f of BMF in beam V3-R4-S1 decreased the crack width at service by 62.81%. In addition, the results showed that BMF had enhanced the load–strain and load–deflection responses of the tested beams (Figs. 13(a) and 14(a)). For example, beam V2-R4-S1 reported

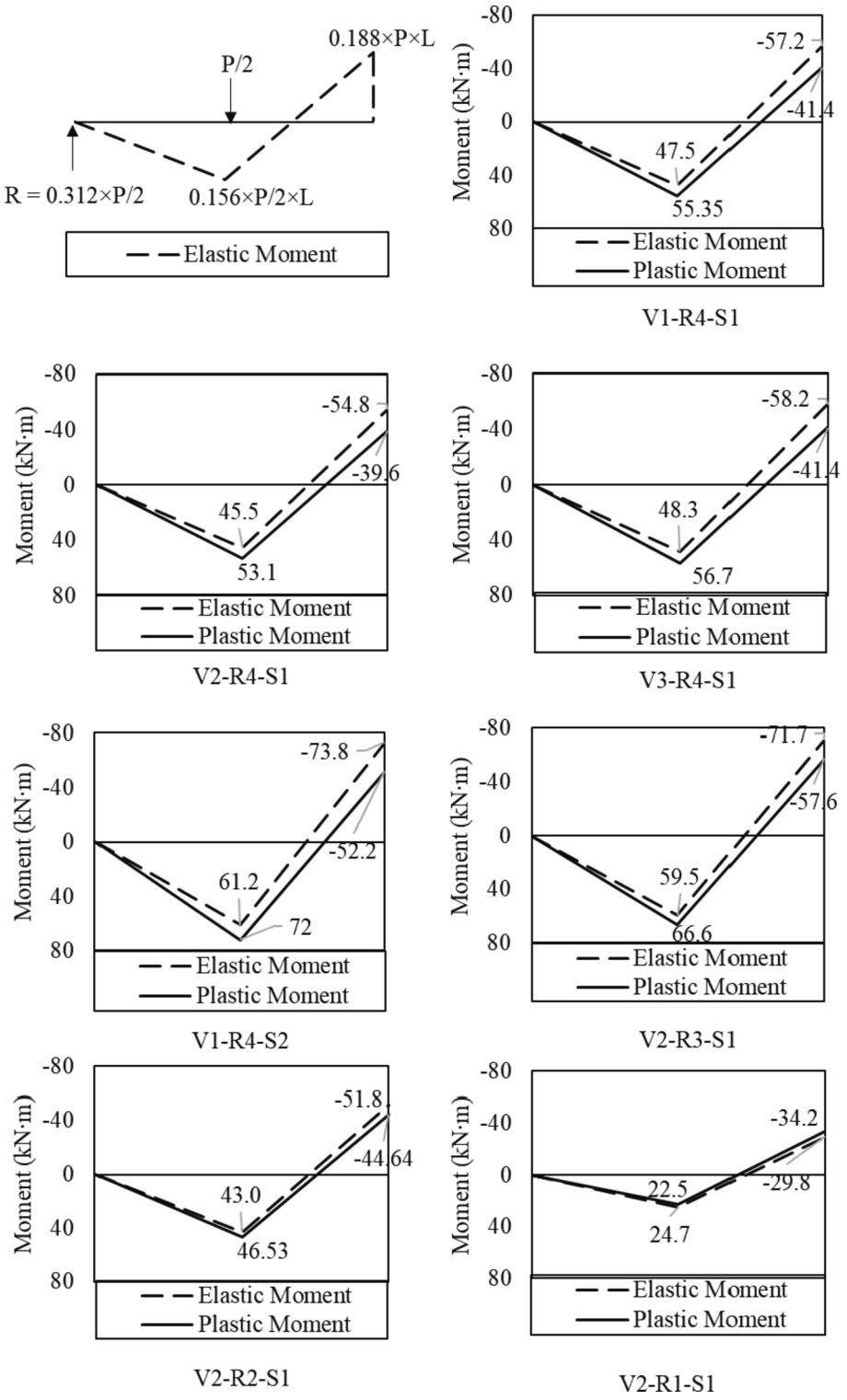

Fig. 15. Elastic versus actual bending moments at failure.

49% and 37% lower tensile strain and mid-span deflection at service than beam V1-R4-S1, respectively. Beam V3-R4-S1 showed a similar trend to that of V2-R4-S1. Furthermore, load-midspan deflection curves in Fig. 14(a) show that the energy absorption capacity of BFRC beams was improved by adding BMF. This improvement was due to the bridging effect of the BMF, which absorbed part of the applied stresses and bridged the initiated cracks. A similar trend was observed by Abed and Alhafiz [44] and Alnahhal and Aljidda [62]. Regarding the effect of BMF on the moment redistribution of the beams, Fig. 15 depicts that beams V1-R4-S1, V2-R4-S1, and V3-R4-S1 achieved 16.5%, 16.7%, and 17.40% sagging moment redistribution and 27.6%, 27.7%, and 28.9% hogging moment redistribution, indicating that the BMF increased the rotational capacity and improved the moment redistribution of the beams. Similarly, Abed and Alhafiz [44] reported that RC beams made with basalt fibers had higher ductility than reference beams with no fibers.

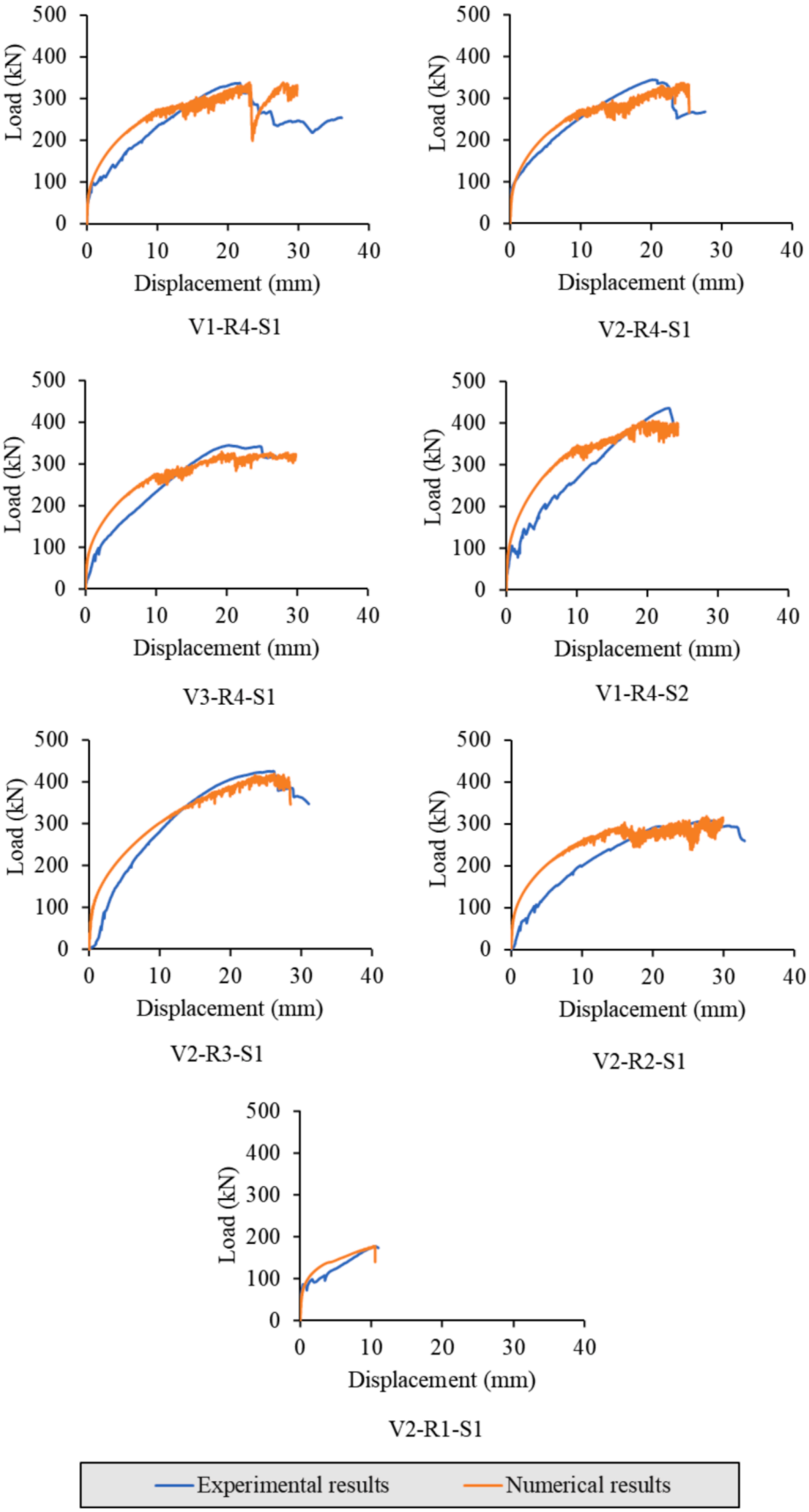

Fig. 16. Predicted and experimental load–displacement responses.

Table 6
Comparison between experimental and predicted ultimate loads and mid-span deflections.

Beam	Ultimate load			Ultimate mid-span deflection		
	Experimental(kN)	Predicted (kN)	Experimental/Predicted	Experimental (mm)	Predicted (mm)	Experimental/Predicted
V1-R4-S1	337	333	1.012	23.48	23.23	1.011
V2-R4-S1	341	336	1.015	22.56	24.19	0.933
V3-R4-S1	345	329	1.049	20.34	19.29	1.054
V1-R4-S2	435	389	1.118	23.09	24.32	0.949
V2-R3-S1	425	405	1.049	26.06	25.68	1.015
V2-R2-S1	308	305	1.010	28.59	29.85	0.958
V2-R1-S1	177	177	1.000	10.65	10.30	1.034
Mean			1.036			0.993
SD			0.041			0.046
COV%			3.950			4.680

4.1.2. Effect of reinforcement ratio

By referring to Table 5, it could be seen that beam V2-R1-S1 failed because of BFRP bar rupture without a sign of crack widening. This is due to the low axial stiffness at the sagging section, which, in turn, decreased its tensile strength capacity. However, increasing the sagging reinforcement ratio in beam V2-R4-S1 increased the beam's stiffness and changed the failure mode from brittle failure to a flexural-compression failure (i.e., concrete crushing). The presented results also revealed that the tested beams' crack widths and strains decreased as the sagging-to-hogging reinforcement ratio increased (Figs. 12(b) and 13(b)). This can be seen in beam V2-R4-S1 that had 68.16% and 20% lower crack widths than beam V2-R2-S1 at service and failure loads, respectively. As well, beam V2-R3-S1 exhibited about 58% lower tensile strain at service than beams V2-R2-S1 and V2-R1-S1. Moreover, Fig. 14(b) shows that increasing hogging and sagging reinforcement ratios enhanced the tested beams' stiffness. For instance, beam V2-R3-S1 exhibited a 28% higher failure load than beam V2-R4-S1. At failure, beams V2-R3-S1, V2-R4-S1, and V2-R2-S1 reported 54%, 39%, and 24% lower deflections than beam V2-R1-S1, respectively. However, beam V2-R1-S1, which was under-reinforced, reported the highest crack widths, strains, and mid-span deflections at all loads compared to all tested beams. The improvement in the crack widths, strains, stiffness by increasing reinforcement ratios can be linked to the increased axial stiffness of BFRP bars, which increased beams' flexural capacity and enhanced the adhesive force between BFRP reinforcing bars and concrete. These findings are consistent with the findings of Akiel et al. [28]. It could also be recognized from the presented results that higher moment redistribution was reported in beams having higher sagging reinforcement ratios (Fig. 15). For instance, beam V2-R3-S1 had 43.11% higher sagging and hogging moment redistribution at failure than beam V2-R2-S1, owing to the increased sagging moment capacity, and thus allowed it to accept more tensile stresses. Conversely, increasing the hogging reinforcement ratio in beam V2-R3-S1 decreased the moment redistribution at failure by 28.94% compared to beam V2-R4-S1. This reduction might be due to the increased flexural rigidity of the hogging section, which allowed it to sustain more tensile stresses and thus decreased the tensile stress transfer toward the sagging section. On the other hand, beam V2-R1-S1, which was under-reinforced in the sagging section, exhibited an inverse moment redistribution (i.e., toward the hogging section). This might have occurred because of the excessive flexural cracks that appeared at the sagging section, consequently decreasing its stiffness. El-Mogy et al. [26] and Akiel et al. [28] also reported an inverse moment redistribution in FRP-RC beams by increasing the hogging reinforcement.

4.1.3. Effect of stirrups spacing

Test results revealed that decreasing the stirrups spacing from 120 to 80 mm in beam V1-R4-S2 changed the failure mode from brittle-shear failure to concrete crushing. Additionally, decreasing the stirrups spacing in beam V1-R4-S2 decreased its crack width, tensile strain, and mid-span deflection at failure by 19%, 40%, and 38%, respectively, in comparison with beam V1-R4-S1 (Figs. 12(c), 13(c), and 14(c)). This is primarily attributed to the effect of the additional stirrups, which absorbed more tensile stresses and increased concrete confinement. It could also be observed from Fig. 15 that stirrups spacing had a minimal effect on the beams' moment redistribution. Beam V1-R4-S2 showed only a 6% increase in the moment redistribution compared to its counterpart with 120 mm stirrups spacing. The slight improvement in the moment redistribution with closer stirrups spacing might be because stirrups are mainly used to resist shear forces.

4.2. Validation of the FE models

The developed FE models were validated using the experimental load–deflection responses and cracking patterns presented in Section 4.1. Fig. 16 showed the load versus mid-span deflection responses at all loading stages for all FE models and their corresponding experimental results. It could be seen that the predicted and experimental load–deflection curves exhibited approximately a bilinear relationship. Similar to the experimental load–deflection curves, the predicted curves showed a quasi-linear relationship up to concrete cracking. After cracking, the curves abruptly and nonlinearly increased with the applied loads because of the stiffness deterioration. The FE models accurately predicted the post cracking behavior and crushing loads of the beams. It could also be observed that the predicted load–deflection curves before failure were slightly stiffer than those obtained experimentally. This might have occurred because the FE analysis assumes a full efficiency, perfectly fit and bonded, and optimal compliance for concrete element, whereas in reality, concrete might be encountered to shrinkage cracks, voids, or extra water, which results in a local degradation in concrete. Similarly, Attia et al. [47] and Metwally [72] reported that the predicted load–deflection curves were stiffer than the experimental ones. A comparison between the predicted and experimental ultimate loads and their corresponding mid-span deflections between FE and experimental results is shown in Table 6. From the table, it is evident that the FE models accurately predicted both ultimate loads and mid-span deflections with a mean, standard deviation (SD), and coefficient of variance (COV) experimental-to-predicted of 1.036, 0.041, and 3.95% for ultimate loads and 0.993, 0.046, and 4.68% for mid-span deflections. In addition, Fig. 17 compares the predicted and experimental crack patterns at failure for the seven beam specimens. It could be seen that FE models have correctly predicted the cracking patterns and damages of the tested beams. Considering these results, the validated FE models can be utilized to predict the response of BFRP-BFRC continuous beams while examining a broader range of parameters as an alternative to experimental tests. However, caution should be paid when utilizing this FE model to other beams' configurations or other types of FRP bars or when different materials are used. Therefore, More experimental data are required to provide more confidence in the developed FE to be used as a powerful tool to study the behavior of BFRP-BFRC continuous beams.

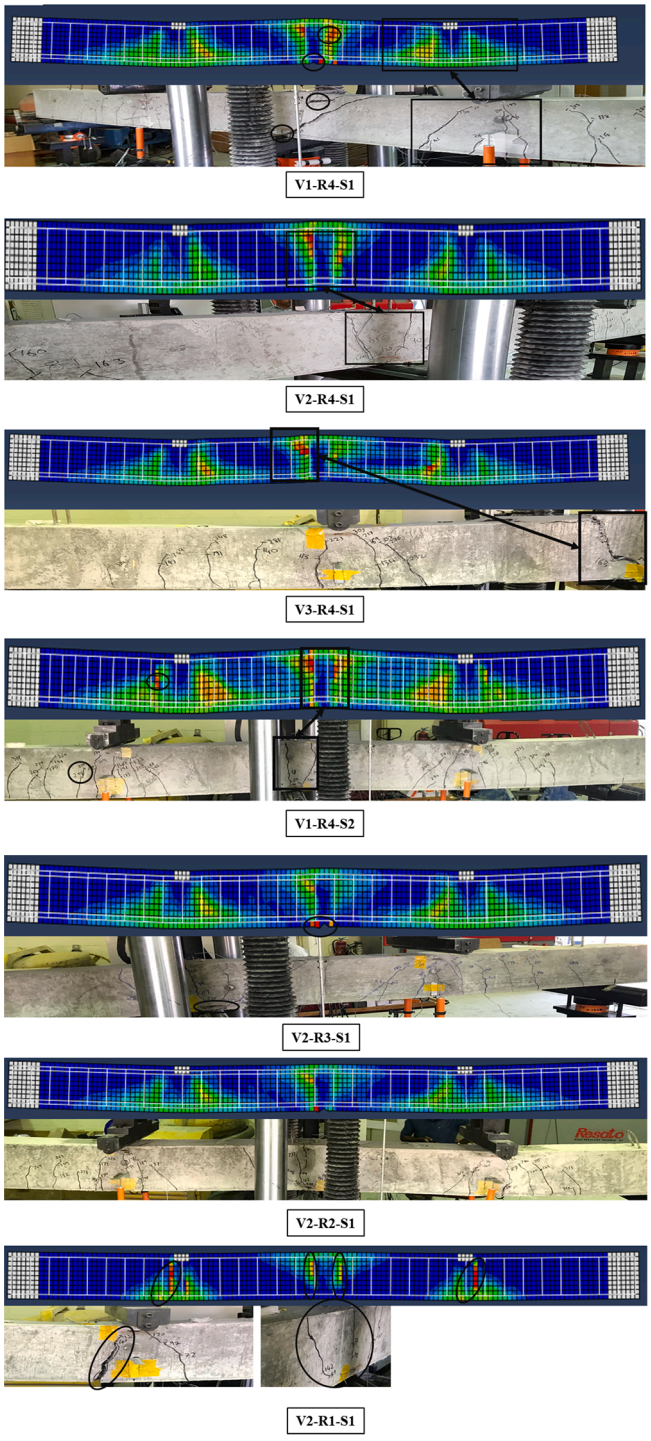

Fig. 17. Predicted and experimental crack patterns of the beams.

5. Conclusions

The structural behavior and moment redistribution of seven BFRP-BFRC continuous beams with different V_f of BMF, reinforcement ratio, and stirrups spacing were experimentally and numerically examined. A total of seven nonlinear 2D FE models were developed to predict the structural behavior of the BFRP-BFRC tested continuous beams. The beams' load–deflection responses and crack patterns were predicted using FE numerical simulations. The main observations and conclusions of this study were drawn as follows:

1- BMF have proved their efficiency in enhancing the flexural strength of concrete. BFRC specimens at V_f of 0.75% and 1.5% reported 5% and 26% higher flexural tensile strength and 14% and 35% higher direct tensile strength than plain concrete specimens, respectively. Furthermore, adding BMF to concrete has changed the failure mode of the flexural prisms from brittle failure to a more ductile failure.
2- The addition of BMF to concrete has changed the tested beams' failure mode from brittle-shear failure to a flexural-compression failure mode (i.e., concrete crushing). Also, BMF have decreased the tested beams' crack widths and strains up to 62% and 49%, respectively, compared to their counterparts with no added BMF.
3- The beams' flexural strength and stiffness were improved by increasing sagging and hogging reinforcement ratios. Increasing the sagging BFRP reinforcement ratio increased the moment redistribution by 43.11%, while increasing the hogging reinforcement ratio decreased the moment redistribution by 28.94%.
4- Decreasing the stirrups spacing has marginally affected the beams' moment redistribution. Further studies are needed to confirm this.
5- Ayub's analytical model provided a reasonable prediction of the behavior of BFRC in compression.
6- The developed FE models accurately predicted the beams' load–deflection responses, with a mean, standard deviation, and coefficient of variance experimental-to-predicted of 1.036, 0.041, and 3.95% for the ultimate loads and 0.993, 0.046, 4.68% for the ultimate deflections, respectively. Moreover, the FE models accurately predicted the beams' cracking patterns and damage locations.

Finally, the current study has confirmed the efficiency of BMF in enhancing the structural behavior of BFRP-BFRC continuous beams in terms of cracking, failure loads, deflections, strains, and moment redistribution. Further studies are still needed to confirm the durability and long-term behavior of BFRP-BFRC elements.

Declaration of Competing Interest

The authors declare that they have no known competing financial interests or personal relationships that could have appeared to influence the work reported in this paper.

Acknowledgment

This publication was made possible by GSRA grant GSRA6-1-0509-19022 from the Qatar National Research Fund (QNRF, a member of Qatar Foundation). The authors also show their gratitude to Qatar University for their financial support through internal research grants no. QUST-1-CENG-2020-17. The findings achieved herein are solely the responsibility of the authors.

Data availability

The raw/processed data required to reproduce these findings cannot be shared at this time as the data also forms part of an ongoing study.

References

[1] Kalfat R, Al-Mahaidi R. Experimental investigation into the size effect of bidirectional fiber patch anchors in strengthening of concrete structures. Compos Struct 2014;112:134–45. https://doi.org/10.1016/j.compstruct.2014.02.011.
[2] Attia K, Alnahhal W, Elrefai A, Rihan Y. Flexural behavior of basalt fiber-reinforced concrete slab strips reinforced with BFRP and GFRP bars. Compos Struct 2019;211:1–12. https://doi.org/10.1016/j.compstruct.2018.12.016.
[3] Hassan M, Benmokrane B, ElSafty A, Fam A. Bond durability of basalt-fiber-reinforced-polymer (BFRP) bars embedded in concrete in aggressive environments. Compos Part B Eng 2016;106:262–72. https://doi.org/10.1016/j.compositesb.2016.09.039.
[4] High C, Seliem HM, El-Safty A, Rizkalla SH. Use of basalt fibers for concrete structures. Constr Build Mater 2015;96:37–46. https://doi.org/10.1016/j.conbuildmat.2015.07.138.

[5] Cai J, Pan J, Zhou X. Flexural behavior of basalt FRP reinforced ECC and concrete beams. Constr Build Mater 2017;142:423–30. https://doi.org/10.1016/J.CONBUILDMAT.2017.03.087.

[6] Elgabbas F, Ahmed EA, Benmokrane B. Flexural behavior of concrete beams reinforced with ribbed basalt-FRP bars under static loads. J Compos Constr 2017;21(3):04016098. https://doi.org/10.1061/(ASCE)CC.1943-5614.0000752.

[7] Atutis M, Valivonis J, Atutis E. Experimental study of concrete beams prestressed with basalt fiber reinforced polymers. Part I : flexural behavior and serviceability. Compos Struct 2018;183:114–23. https://doi.org/10.1016/j.compstruct.2017.01.081.

[8] Tomlinson D, Fam A. Performance of concrete beams reinforced with basalt FRP for flexure and shear. J Compos Constr 2015;19(2):04014036. https://doi.org/10.1061/(ASCE)CC.1943-5614.0000491.

[9] El Refai A, Abed F. Concrete contribution to shear strength of beams reinforced with basalt fiber-reinforced bars. J Compos Constr 2016;20(4):04015082. https://doi.org/10.1061/(ASCE)CC.1943-5614.0000648.

[10] Taha A, Alnahhal W, Alnuaimi N. Bond durability of basalt FRP bars to fiber reinforced concrete in a saline environment. Compos Struct 2020;243:112277. https://doi.org/10.1016/j.compstruct.2020.112277.

[11] El Refai A, Ammar M-A, Masmoudi R. Bond performance of basalt fiber-reinforced polymer bars to concrete. J Compos Constr 2015;19(3):04014050. https://doi.org/10.1061/(ASCE)CC.1943-5614.0000487.

[12] Yang Y, Li Z, Zhang T, Wei J, Yu Q. Bond-slip behavior of basalt fiber reinforced polymer bar in concrete subjected to simulated marine environment: effects of BFRP bar size, corrosion age, and concrete strength. Int J Polym Sci 2017;2017:1–9. https://doi.org/10.1155/2017/5156189.

[13] El Refai A, Abed F, Altalmas A. Bond durability of basalt fiber-reinforced polymer bars embedded in concrete under direct pullout conditions. J Compos Constr 2015;19(5):04014078. https://doi.org/10.1061/(ASCE)CC.1943-5614.0000544.

[14] Li C, Gao D, Wang Y, Tang J. Effect of high temperature on the bond performance between basalt fibre reinforced polymer (BFRP) bars and concrete. Constr Build Mater 2017;141:44–51. https://doi.org/10.1016/j.conbuildmat.2017.02.125.

[15] Altalmas A, El Refai A, Abed F. Bond degradation of basalt fiber-reinforced polymer (BFRP) bars exposed to accelerated aging conditions. Constr Build Mater 2015;81:162–71. https://doi.org/10.1016/J.CONBUILDMAT.2015.02.036.

[16] Liu H, Yang J, Wang X. Bond behavior between BFRP bar and recycled aggregate concrete reinforced with basalt fiber. Constr Build Mater 2017;135:477–83. https://doi.org/10.1016/j.conbuildmat.2016.12.161.

[17] Xiong Z, Wei W, Liu F, Cui C, Li L, Zou R, et al. Bond behaviour of recycled aggregate concrete with basalt fibre-reinforced polymer bars. Compos Struct 2021;256:113078. https://doi.org/10.1016/j.compstruct.2020.113078.

[18] Piotr D, Krzysztof K. Research in redistribution of bending moments in the beams of reinforced concrete early loaded. Procedia Eng 2017;172:883–90. https://doi.org/10.1016/j.proeng.2017.02.096.

[19] Bagge N, O'Connor A, Elfgren L, Pedersen C. Moment redistribution in RC beams – a study of the influence of longitudinal and transverse reinforcement ratios and concrete strength. Eng Struct 2014;80:11–23. https://doi.org/10.1016/j.engstruct.2014.08.029.

[20] Kodur VKR, Campbell TI. Evaluation of moment redistribution in a two-span continuous prestressed concrete beam. ACI Struct J 1996;93. https://doi.org/10.14359/519.

[21] Moment and Shear Redistribution in Two-Span Continuous Reinforced Concrete Beams*. ACI J Proc 1958;55. https://doi.org/10.14359/11375.

[22] Mahroug MEM, Ashour AF, Lam D. Tests of continuous concrete slabs reinforced with carbon fibre reinforced polymer bars. Compos Part B Eng 2014;66:348–57. https://doi.org/10.1016/j.compositesb.2014.06.003.

[23] Unsal I, Tokgoz S, Çağatay İ, Dundar C. A study on load-deflection behavior of two-span continuous concrete beams reinforced with GFRP and steel bars. Struct Eng Mech 2017;63:629–37. https://doi.org/10.12989/sem.2017.63.5.629.

[24] Habeeb MN, Ashour AF. Flexural behavior of continuous GFRP reinforced concrete beams. J Compos Constr 2008;12(2):115–24. https://doi.org/10.1061/(ASCE)1090-0268(2008)12:2(115).

[25] El-Mogy M, El-Ragaby A, El-Salakawy E. Effect of transverse reinforcement on the flexural behavior of continuous concrete beams reinforced with FRP. J Compos Constr 2011;15(5):672–81. https://doi.org/10.1061/(ASCE)CC.1943-5614.0000215.

[26] El-Mogy M, El-Ragaby A, El-Salakawy E. Flexural behavior of continuous FRP-reinforced concrete beams. J Compos Constr 2010;14(6):669–80. https://doi.org/10.1061/(ASCE)CC.1943-5614.0000140.

[27] Rahman SMH, Mahmoud K, El-Salakawy E. Moment redistribution in glass fiber reinforced polymer-reinforced concrete continuous beams subjected to unsymmetrical loading. Eng Struct 2017;150:562–72. https://doi.org/10.1016/j.engstruct.2017.07.066.

[28] Akiel MS, El-Maaddawy T, El Refai A. Serviceability and moment redistribution of continuous concrete members reinforced with hybrid steel-BFRP bars. Constr Build Mater 2018;175:672–81. https://doi.org/10.1016/j.conbuildmat.2018.04.202.

[29] Mahroug MEM, Ashour AF, Lam D. Experimental response and code modelling of continuous concrete slabs reinforced with BFRP bars. Compos Struct 2014;107:664–74. https://doi.org/10.1016/J.COMPSTRUCT.2013.08.029.

[30] ACI (American Concrete Institute Committee 440). Guide for the Design and Construction of Structural Concrete Reinforced with Fibre-Reinforced Polymer (FRP) Bars. (ACI 4401R-15) 2015. https://doi.org/10.1061/40753(171)158.

[31] JSCE(Japan Society of Civil Engineers). Recommendation for design and construction of concrete structures using continuous fiber reinforcing materials. 1997:1–58.

[32] CSA (Canadian Standards Association). Design and construction of building components with fiber reinforced polymers. (CSA-S806-12) 2012.

[33] ISIS (Intelligent Sensing for Innovative Structures). Reinforcing Concrete Structures with Fibre Reinforced Polymers; 2007.

[34] Rahman SMH, Mahmoud K, El-Salakawy E. Behavior of glass fiber-reinforced polymer reinforced concrete continuous T-beams. J Compos Constr 2017;21(2):04016085. https://doi.org/10.1061/(ASCE)CC.1943-5614.0000740.

[35] Gravina RJ, Smith ST. Flexural behaviour of indeterminate concrete beams reinforced with FRP bars. Eng Struct 2008;30(9):2370–80. https://doi.org/10.1016/j.engstruct.2007.12.019.

[36] Razaqpur AG, Mostofinejad D. Experimental Study of Shear Behavior of Continuous Beams Reinforced with Carbon Fiber Reinforced Polymer. In: Dolan CW, Rizkalla SH, Nanni A, editors. 4th Int. Symp., Fiber Reinf. Polym. Reinf. Reinf. Concr. Struct., vol. 188, 1999, p. 169–78.

[37] Santos P, Laranja G, França PM, Correia JR. Ductility and moment redistribution capacity of multi-span T-section concrete beams reinforced with GFRP bars. Constr Build Mater 2013;49:949–61. https://doi.org/10.1016/j.conbuildmat.2013.01.014.

[38] Yang J-M, Min K-H, Shin H-O, Yoon Y-S. Effect of steel and synthetic fibers on flexural behavior of high-strength concrete beams reinforced with FRP bars. Compos Part B Eng 2012;43(3):1077–86. https://doi.org/10.1016/j.compositesb.2012.01.044.

[39] Wang H, Belarbi A. Ductility characteristics of fiber-reinforced-concrete beams reinforced with FRP rebars. Constr Build Mater 2011;25(5):2391–401. https://doi.org/10.1016/j.conbuildmat.2010.11.040.

[40] Issa MS, Metwally IM, Elzeiny SM. Influence of fibers on flexural behavior and ductility of concrete beams reinforced with GFRP rebars. Eng Struct 2011;33(5):1754–63. https://doi.org/10.1016/j.engstruct.2011.02.014.

[41] Soltanzadeh F, Behbahani AE, Mazaheripour H, Barros JAO. Shear resistance of SFRSCC short-span beams without transversal reinforcements. Compos Struct 2016;139:42–61. https://doi.org/10.1016/J.COMPSTRUCT.2015.11.067.

[42] Abed F, Alhafiz AR. Effect of basalt fibers on the flexural behavior of concrete beams reinforced with BFRP bars. Compos Struct 2019;215:23–34. https://doi.org/10.1016/j.compstruct.2019.02.050.

[43] Wang H, Belarbi A. Flexural durability of FRP bars embedded in fiber-reinforced-concrete. Constr Build Mater 2013;44:541–50. https://doi.org/10.1016/J.CONBUILDMAT.2013.02.065.

[44] Abed F, Rahman A. Effect of basalt fibers on the flexural behavior of concrete beams reinforced with BFRP bars 2019;215:23–34. https://doi.org/10.1016/j.compstruct.2019.02.050.

[45] Lee WK, Jansen DC, Berlin KB, Cohen IE. Flexural cracks in Fiber-reinforced concrete beams with Fiber-reinforced polymer reinforcing bars. ACI Struct J 2010;107:321–9.

[46] Visintin P, Mohamad Ali MS, Xie T, Sturm AB. Experimental investigation of moment redistribution in ultra-high performance fibre reinforced concrete beams. Constr Build Mater 2018;166:433–44. https://doi.org/10.1016/j.conbuildmat.2018.01.156.

[47] Attia K, El Refai A, Alnahhal W. Flexural behavior of basalt fiber-reinforced concrete slab strips with BFRP bars: experimental testing and numerical simulation. J Compos Constr 2020;24(2):04020007. https://doi.org/10.1061/(ASCE)CC.1943-5614.0001002.

[48] Behnam H, Kuang JS, Samali B. Parametric finite element analysis of RC wide beam-column connections. Comput Struct 2018;205:28–44. https://doi.org/10.1016/j.compstruc.2018.04.004.

[49] Lin F, Zhong Q, Zhang Z. Flexural behaviour of RC beams reinforced with compressive steel bars and two-piece enclosed stirrups. Constr Build Mater 2016;126:55–65. https://doi.org/10.1016/j.conbuildmat.2016.09.016.

[50] Haido JH. Flexural behavior of basalt fiber reinforced concrete beams: finite element simulation with new constitutive relationships. Structures 2020;27:1876–89. https://doi.org/10.1016/j.istruc.2020.08.005.

[51] Sun X, Gao Z, Cao P, Zhou C, Ling Y, Wang X, et al. Fracture performance and numerical simulation of basalt fiber concrete using three-point bending test on notched beam. Constr Build Mater 2019;225:788–800. https://doi.org/10.1016/j.conbuildmat.2019.07.244.

[52] Pawłowski D, Szumigała M. Flexural behaviour of full-scale basalt FRP RC beams – experimental and numerical studies. Procedia Eng 2015;108:518–25. https://doi.org/10.1016/j.proeng.2015.06.114.

[53] Adam MA, Said M, Mahmoud AA, Shanour AS. Analytical and experimental flexural behavior of concrete beams reinforced with glass fiber reinforced polymers bars. Constr Build Mater 2015;84:354–66. https://doi.org/https://doi.org/10.1016/j.conbuildmat.2015.03.057.

[54] Wang T, Hsu TTC. Nonlinear finite element analysis of concrete structures using new constitutive models. Comput Struct 2001;79(32):2781–91. https://doi.org/10.1016/S0045-7949(01)00157-2.

[55] Standard Test Method for Slump of Hydraulic-Cement Concrete. ASTM C143/C143M-15a 2015:15–8. https://doi.org/10.1520/C0143_C0143M-15A.

[56] Chen B, Liu J. Contribution of hybrid fibers on the properties of the high-strength lightweight concrete having good workability. Cem Concr Res 2005;35(5):913–7. https://doi.org/10.1016/j.cemconres.2004.07.035.

[57] Ramesh B, Eswari S. Mechanical behaviour of basalt fibre reinforced concrete: an experimental study. Mater Today Proc 2021;43:2317–22. https://doi.org/10.1016/j.matpr.2021.01.071.

[58] Standard Test Method for Compressive Strength of Cylindrical Concrete Specimens. ASTM C39/C39M-20 2020:1–8. https://doi.org/10.1520/C0039_C0039M-20.

[59] ASTM C1609/C1609M-12. Standard Test Method for Flexural Performance of Fiber-Reinforced Concrete (Using Beam With Third-Point Loading). 2012. https://doi.org/10.1520/C1609_C1609M-12.
[60] Jiang C, Fan K, Wu F, Chen D. Experimental study on the mechanical properties and microstructure of chopped basalt fibre reinforced concrete. Mater Des 2014; 58:187–93. https://doi.org/10.1016/j.matdes.2014.01.056.
[61] Branston J, Das S, Kenno SY, Taylor C. Mechanical behaviour of basalt fibre reinforced concrete. Constr Build Mater 2016;124:878–86. https://doi.org/10.1016/J.CONBUILDMAT.2016.08.009.
[62] Alnahhal W, Aljidda O. Flexural behavior of basalt fiber reinforced concrete beams with recycled concrete coarse aggregates. Constr Build Mater 2018;169:165–78. https://doi.org/10.1016/j.conbuildmat.2018.02.135.
[63] Abaqus 6.14 Documentation 2014.
[64] Obaidat YT, Heyden S, Dahlblom O. The effect of CFRP and CFRP / concrete interface models when modelling retrofitted RC beams with FEM. Compos Struct 2010;92(6):1391–8. https://doi.org/10.1016/j.compstruct.2009.11.008.
[65] Alfarah B, López-Almansa F, Oller S. New methodology for calculating damage variables evolution in plastic damage model for RC structures. Eng Struct 2017; 132:70–86. https://doi.org/10.1016/j.engstruct.2016.11.022.
[66] Mirza O, Uy B. Behaviour of headed stud shear connectors for composite steel–concrete beams at elevated temperatures. J Constr Steel Res 2009;65(3): 662–74. https://doi.org/10.1016/j.jcsr.2008.03.008.
[67] Navarro M, Ivorra S, Varona FB. Parametric finite element analysis of punching shear behaviour of RC slabs reinforced with bolts. Comput Struct 2020;228: 106147. https://doi.org/10.1016/j.compstruc.2019.106147.
[68] Mosallam A, Allam K, Salama M. Analytical and numerical modeling of RC beam-column joints retrofitted with FRP laminates and hybrid composite connectors. Compos Struct 2019;214:486–503. https://doi.org/10.1016/j.compstruct.2019.02.032.
[69] Tao Y, Chen JF, Asce M. Concrete damage plasticity model for modeling FRP-to-concrete bond behavior. J Comp Constr 2014:1–13. https://doi.org/10.1061/(ASCE)CC.1943-5614.0000482.
[70] Genikomsou AS, Polak MA. Damaged plasticity modelling of concrete in finite element analysis of reinforced concrete slabs. 9th Int. Conf. Fract. Mech. Concr. Concr. Struct., 2016. https://doi.org/10.21012/FC9.006.
[71] Ayub T, Khan SU, Shafiq N. Flexural modelling and finite element analysis of FRC beams reinforced with PVA and basalt fibres and their validation. Adv Civ Eng 2018;2018:1–18. https://doi.org/10.1155/2018/8060852.
[72] Metwally IM. Three-dimensional nonlinear finite element analysis of concrete deep beam reinforced with GFRP bars. HBRC J 2017;13(1):25–38. https://doi.org/10.1016/j.hbrcj.2015.02.006.